On the improvement of chemical conversion in a surface-wave microwave plasma reactor for CO_2 reduction with hydrogen (The Reverse Water-Gas Shift reaction)

Fernández de la Fuente, Javier; Moreno Wandurraga, Sergio; Stankiewicz, Andrzej; Stefanidis, Georgios

DOI
10.1016/j.ijhydene.2017.04.040

Publication date
2017

Document Version
Accepted author manuscript

Published in
International Journal of Hydrogen Energy

Link to formal publication International Journal of Hydrogen Energy (Elsevier): https://doi.org/10.1016/j.ijhydene.2017.04.040

On the improvement of chemical conversion in a surface-wave microwave plasma reactor for CO_2 reduction with hydrogen (The Reverse Water-Gas Shift reaction)

Javier F. de la Fuente[1], Sergio H. Moreno[1], Andrzej I. Stankiewicz[1] and Georgios D. Stefanidis[2,*]

[1] *Intensified Reaction & Separation Systems, Process & Energy Laboratory, Delft University of Technology, Leeghwaterstraat 39, 2628 CB, Delft, The Netherlands*

[2] *Chemical Engineering Department, Katholieke Universiteit Leuven, Celestijnenlaan 200f, 3001 Leuven (Heverlee), Belgium*

* Corresponding author: Georgios D. Stefanidis, e-mail: georgios.stefanidis@cit.kuleuven.be

Abstract

A novel surface-wave microwave discharge reactor configuration to generate syngas via gaseous CO_2 reduction with H_2 (non-catalytic Reverse Water-Gas Shift reaction) is studied in the context of power-to-chemicals concept. Improvement of CO_2 conversion to maximize CO production is explored by adding an external cylindrical waveguide downstream of the plasma generation system. A 2D self-consistent argon model shows that power absorption and plasma uniformity are improved in the presence of the waveguide. We show experimentally that CO_2 conversion is increased by 50% (from 40% to 60%) at the stoichiometric feed ratio H_2:CO_2 equal to 1 when using the waveguide. At higher H_2:CO_2 ratios, the effect of the waveguide on the reactor performance is nearly negligible. Optical emission spectroscopy reveals that the waveguide causes significant increase in the concentration of O atoms at a ratio H_2:CO_2=1. The effects of the operating pressure and cooling rate are also investigated. A minimum CO_2 conversion is found at 75 mbar and ratio H_2:CO_2 = 1, which is in the transition zone where plasma evolves from diffusive to combined operation regime. The cooling rates have significant impact on CO_2 conversion, which points out the importance of carefully designing the cooling system, among other components of the process, to optimize the plasma effectiveness.

Keywords

Microwave plasma, Reverse Water-Gas Shift, CO_2 utilization, power-to-chemicals

1. Introduction

There is an imminent need to reduce the societal dependence on fossil fuels and increase the usage of renewable electricity to mitigate climate change. According to the International Energy Agency (IEA), electricity accounts for less than 25% of the world total energy consumption [1] because sectors such as transportation and industry with high demand for energy still depend strongly on carbonaceous fuels. One solution to increase the share of electricity over the total energy consumption is based on the production of the same energy carriers through chemical pathways in which renewable electricity is used as the energy source. In this regard, three criteria must be satisfied: (1) the manufactured fuels must have a high energy density, (2) handling of fuels must be possible using the current infrastructure, and (3) the production cost must be comparable with or even lower than fossil fuels-based processes [2]. When liquid fuels, such as alcohols [3], gasoline or diesel, are produced, the first two of the aforementioned requirements are fulfilled because these liquid fuels can be easily transported and stored. The biggest challenge concerns the manufacturing cost of fuels produced via renewable energy; to date, none of the technologies under development has made a breakthrough to achieve competitive production costs compared to the processes using fossil fuels [4-7]. Therefore, further improvement on the overall efficiency of electricity-based systems is vital for the commercial implementation of power-to-chemicals approaches [8, 9].

It is interesting to explore the production of solar fuels (oxygenates, hydrocarbons) from CO_2 and solar hydrogen, i.e. hydrogen produced via water electrolysis using electricity from renewable energy sources, due to the much larger demand (14 times) for hydrocarbons compared to other non-fuel chemicals [10,11]. The Reverse Water-Gas Shift (RWGS) reaction is a key intermediate step to produce high added-value products using CO_2 as feedstock. The main product of this reaction is synthesis gas (mixture of CO and (unreacted) H_2), which can be used, after further adjustment of the H_2/CO ratio downstream, to produce other chemicals through the Fischer-Tropsch process [12]. In this regard, plasma-assisted reactors are key players in the development of electricity-based technologies. Microwave plasma (MWP) is considered one of the most promising alternatives due to various benefits that have been widely discussed in the literature [13-17]. Particularly, travelling-wave-sustained discharges are investigated because of the flexible operation regimes (continuous wave and pulse), the broad attainable pressure range (10^{-5} torr – 1 atm) and wave-frequency range (f = 500 kHz – 10 GHz), as well as wide plasma reactor size range in cylindrical reactor

configurations (R = 0.5 mm – 15 cm) [18]. Moreover, this type of discharge production systems can create large plasma volumes and enable scale-up of MWP reactors for gas processing applications. To find the optimum chemical conversion and energy efficiency, various parameters should be considered in the optimization process: input power, throughput, feed composition, pressure, cooling rates and frequency along with the reactor material, geometry & size. Furthermore, it is essential to understand the interaction of electromagnetic waves with the plasma in order to enhance overall reactor performance. More information on surface-wave (SW) discharges can be found in [18-21].

Two approaches can be considered when aiming to improve the chemical conversion and/or energy efficiency of MWP reactors: (1) the invasive approach, such as the alteration of the plasma reactor geometry to attain certain flow regimes or the addition of (a) alkali metal coated surfaces or (b) catalysts [22] to optimize plasma conditions, and (2) the non-invasive approach, where external elements or fields are applied to the reactor in order to produce more uniform and stable plasmas [16]. One example of the former approach is given by Bongers et al. [23], where different reactor geometries and configurations (forward and reverse vortex, supersonic plasma expansion, quenching tube) were investigated to boost the energy efficiency of the CO_2 splitting process by rapidly cooling the molecules to avoid recombination reactions. Van Rooij et al. [24] proposed to add a coating of low ionization potential alkali metals (lithium or sodium) to, among other effects, lower the electron temperature in order to promote the dissociation of CO_2 molecules via vibrational excitation. Bhattacharya et al. [25] studied a similar concept for the use of microwaves to reduce the energy consumption for endothermic reactions by including a metallic coating on the reactor wall, which brought about significant energy savings. Concerning the second (non-invasive) approach, Spencer et al. [26] made use of two bronze waveguides upstream and downstream of the plasma ignition zone to investigate CO_2 splitting, but its effect on the reactor performance was not reported.

In this work, we present modelling and experimental results of a SW sustained microwave discharge in which the process performance of two different reactor configurations is assessed. A cylindrical waveguide attached to the downstream reactor section is implemented to evaluate its potential to increase the absorption of microwave power and enlarge the plasma reaction zone. A 2D self-consistent argon microwave plasma model gives insight into the spatially-resolved plasma and wave properties (electric field, electron density and

temperature), which allows for evaluation of the plasma behaviour. Experimental results for the reverse-water-gas-shift (RWGS) reaction shows the influence of the waveguide on the process performance. The work focuses on the improvement of CO_2 conversion in the RWGS reaction and on the understanding of the plasma-wave interplay and its effect on reactor performance.

2. Materials and methods

2.1. Novel reactor configuration

The RWGS reaction is explored in a modified version of the SW microwave discharge presented in our previous work [27]. The upgraded bench-scale setup and the gas supply unit are shown in Fig. 1. The core of the equipment is the same as the one previously used, and comprises: (1) solid-state microwave generator (MiniFlow 200SS, Sairem), (2) electromagnetic surface-wave launcher (surfatron 60, Sairem), (3) quartz tube (reactor) with inner and outer diameters of 4 and 5 mm respectively, and (4) vacuum pump (SC920, KNF). With respect to the analytical techniques, mass spectroscopy (QGA Quantitative Gas Analyser, Hiden Analytical), optical emission spectroscopy (OES; MAYA2000PRO, Ocean Optics) and infrared thermography (FLIR A645 SC infrared thermal camera) are used to qualitatively and quantitatively evaluate the plasma performance with two different reactor configurations. Both compressed N_2 and cooling water are used to cool down the surfatron body and the quartz tube outer wall. The operating conditions set in the experiments are: reactants flow rate = 0.1-0.4 l/min, pressure = 20-200 mbar, input microwave power = 60-200 W, feed gas composition H_2:CO_2 = 1-3, cooling N_2 flow rate = 0-40 l/h (T_{in} = 20 ^oC), cooling water flow rate = 0.3 l/min (T_{in} = 6 ^oC), argon flow rate = 5-50 ml/min. As regards the experimental procedure, the first step is plasma ignition, which is carried out at low operating pressures (6-10 mbar), maximum microwave power (200 W) and argon flow rate of 50 ml/min. After plasma is ignited, the reactants (CO_2 + H_2) and argon, as a carrier gas (5 ml/min), are fed to the reactor. Once the reflected power is minimized and plasma is stabilized, the final step involves measuring gas composition, emission spectrum, and infrared image.

In this work, attention was paid to the automation of the system. If MWP reactors are to be implemented at commercial scale for chemical manufacturing applications, several process

aspects must be carefully evaluated; these include (1) safety; the operation of microwave discharges entail the consideration of hazards, such as reactor melting, microwave leakage, and toxic gas leakage (e.g. CO), (2) controllability; operating MWP reactors implies the manipulation and control of a large number of process parameters, which in turn requires the development of highly automated systems, and (3) reproducibility; slight variations of operating conditions can lead to notable changes in the output product, meaning that the installation of accurate measurement devices with rather quick time response is needed to react to the inherently fast dynamics of microwave discharges. In this regard, a semi-automated SW MWP reactor is built, in which hardware such as pneumatic valves operated by compressed air (Fig. 1(a)), gas detection systems, a microwave leakage detector and several pressure and temperature measurement devices and interlocks are installed along the setup. All the aforementioned devices are connected to a CompactRIO controller (National Instruments), which controls real-time applications by means of a LabVIEW interface.

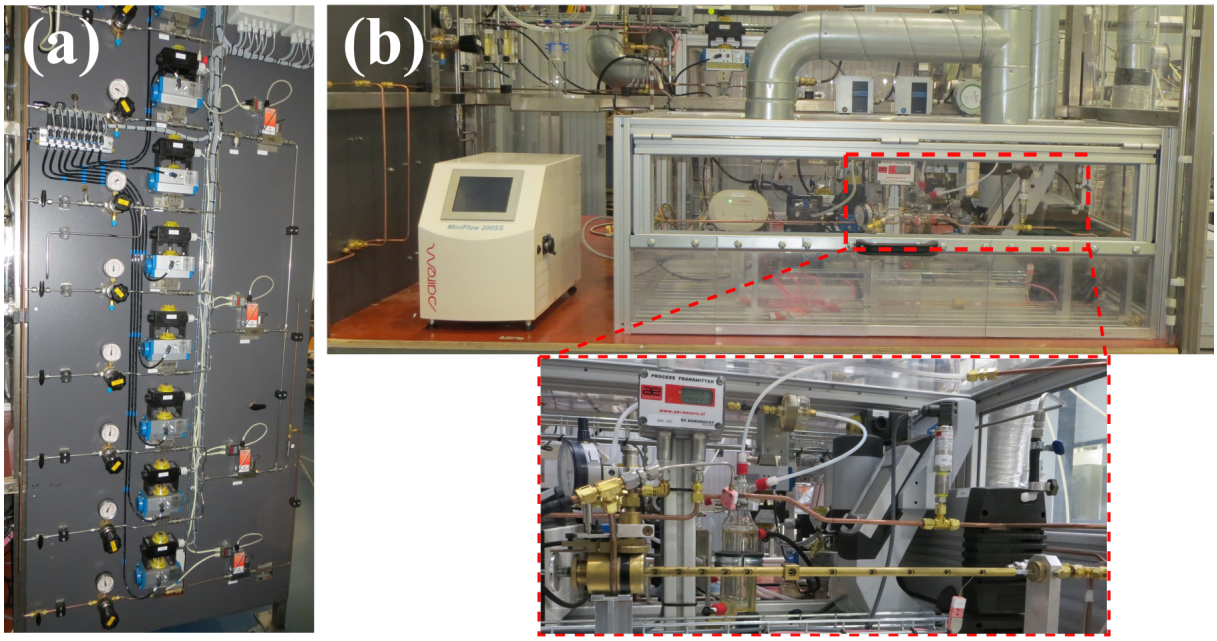

Fig. 1. Schematic of the (a) gas supply unit and (b) the semi-automated bench-scale SW microwave plasma setup.

In addition, an alternative method compared to the one considered in our previous work [27] is used to validate the measurements performed via mass spectroscopy. The method involves calculation of calibration curves by injecting a tiny amount of argon (5 ml/min) in combination with the gas of interest at different mass flow rates. This procedure allows finding a calibration factor that relates the ratio of the partial pressure of each gas to the

partial pressure of argon. The effect of the addition of argon as carrier gas to the plasma is studied by OES, which turned out to have no influence on the intensity of key excited species (OH radical, O and H atoms). For further information on this characterization method, the reader is referred to the references [26, 28].

3. Results and discussion

3.1. Modelling work

To evaluate the effect of an additional cylindrical waveguide on important process parameters such as electromagnetic field distribution, electron density, electron temperature and gas temperature, a 2D axisymmetric self-consistent argon microwave plasma (MWP) model is presented. This model illustrates the variations observed in wave and plasma properties when comparing two reactor configurations: (1) single discharge tube MWP reactor as the one assessed in our earlier work [27], and (2) secondary waveguide-based MWP reactor presented herein. As shortly discussed in the Introduction, several options to enhance the overall process performance in MWP reactors can be proposed. In this work, we opt to explore a non-invasive approach using a cylindrical waveguide to increase absorption of the microwave power. The waveguide redirects back to the discharge a fraction of the energy flux that would otherwise be dissipated to the surroundings [29, 30]. This concept is further evaluated in the following section "Modelling results". Furthermore, the installation of the waveguide not only prevents microwave leakage by encasing the discharge tube, but also facilitates the realization of spatially uniform measurements of emission spectra through 5 mm outer-diameter holes placed axially along the cylindrical waveguide, see Fig. 1(b).

Fig. 2 shows a schematic drawing of the surface-wave (SW) MWP reactor including the secondary waveguide along with the computational domain highlighted in the top section of Fig. 2. In the bottom section of Fig. 2, the 2D axisymmetric geometry used in the simulations is outlined. The computational domain consists of the plasma region (inside the dielectric tube), the quartz (dielectric) tube, the SW launcher (surfatron), where the wave propagation cavity and the microwave excitation port are located, the gas inlet and outlet and the waveguide placed downstream of the plasma generator.

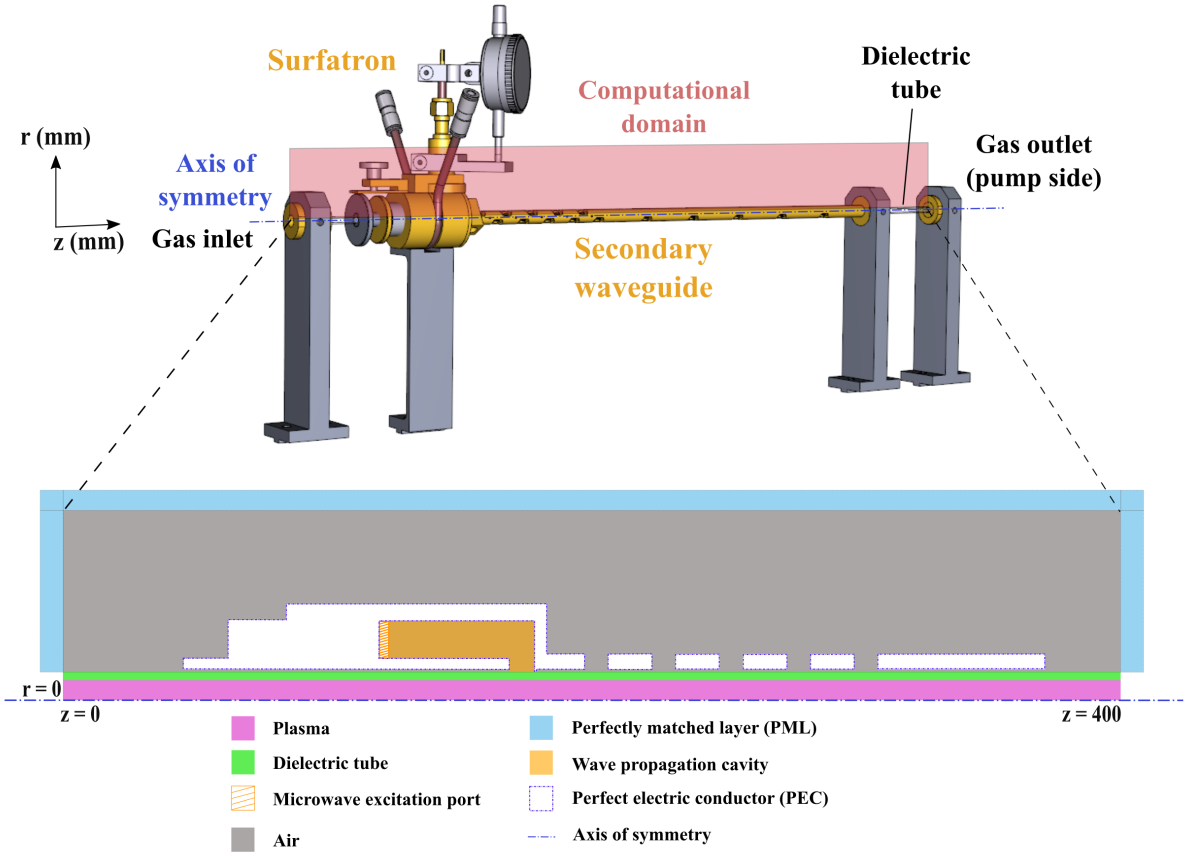

Fig. 2. Schematic drawing of the SW MWP reactor including the reactor configuration, the computational domain and the 2D axisymmetric geometry used in the numerical model.

3.1.1. Description of the model

The argon model of the SW microwave discharge is built in the commercial software COMSOL Multiphysics [31]. The total model accounts for microwave plasma, laminar flow and conductive heat transfer in fluids. The submodels, implemented in respective software modules, are solved self-consistently in a frequency-transient study, which calculates the electromagnetic field in the frequency domain and the remaining variables in the time domain. In this scheme, variations within the microwave cycles are not computed in order to attain steady state solutions in much shorter time. Solution times are in the order of 15-20 min. The multiphysics interface is fully coupled, meaning that it shares parameters or variables between the physics simultaneously. The microwave plasma interface can be considered as the core of the model. It solves the electromagnetic wave equation (including heating of the electrons), the drift-diffusion equations for the conservation of mass and energy of electrons, the heavy species transport equations and the ambipolar field due to space charge separation. Regarding the electromagnetic field, the transverse electromagnetic (TEM) mode

is assumed at the coaxial excitation port. The relative permittivity and permeability are taken from the materials specifications. For the drift-diffusion equations, a Maxwellian electron energy distribution function is specified and the electron transport properties are given in reduced form.

Cross section data is used to determine the electron impact reaction rate coefficients. The mixture-averaged model is used for the mass transport, in which the mixture diffusion coefficient for each species is computed based on the binary diffusion coefficients of the species in the mixture. The thermodynamic and transport properties of the gas mixture are calculated by means of the ideal gas mixture model. Ambipolar diffusion is considered for the charged species. All the reaction kinetics considered in the argon model are presented in Table 1 along with the corresponding references.

Table 1. Reactions included in the model.

No	Process	Reaction	ΔE [eV]	Rate constant	Sticking coefficient	Ref.
1	Elastic scattering	e + Ar→e + Ar	0	$f(E/N)$	N/A	[32]
2	Ground state excitation	e + Ar→e + Ars	11.50	$f(E/N)$	N/A	[32]
3	Superelastic	e + Ars→e + Ar	-11.50	$f(E/N)$	N/A	[a]
4	Ground state ionization	e + Ar→e + e + Ar^+	15.80	$f(E/N)$	N/A	[32]
5	Step-wise ionization	e + Ars→e + e + Ar^+	4.24	$f(E/N)$	N/A	[33]
6	Two-body quenching	Ars + Ar→Ar + Ar	-11.50	1807[b]	N/A	[34]
7	Penning ionization	Ars + Ars→e + Ar + Ar^+	-7.20	3.734·E8[b]	N/A	[35, 36]
8	Quenching[c]	Ars→Ar	N/A	N/A	1	N/A
9	Neutralization[c]	Ar^+→Ar	N/A	N/A	1	N/A

[a] Computed with the detailed balancing principle

[b] Units in [m^3/s·mol]

[c] Surface reactions

N/A: Not applicable

The velocity and pressure fields used as input to the microwave plasma and heat transfer in fluids interfaces are solved by the laminar flow module. This is configured to calculate the Navier-Stokes and continuity equations for a compressible (Mach < 0.3) single-phase laminar flow with the thermodynamic and transport properties taken from the microwave plasma interface. Similarly, the temperature field is computed by the heat transfer in fluids module, which solves the energy conservation and the Fourier's law of heat conduction for a fluid with the thermodynamic and transport properties taken once again from the microwave plasma

interface. Convection and radiation are neglected and the gas heating source is considered to be the sum of the heats of reactions solved by the microwave plasma interface. For additional information on the equations solved, the reader is referred to [19, 30, 37-40].

To date, this model cannot be applied to study the RWGS reaction itself as the available kinetic models for CO_2 and gas mixtures ($CO_2 + H_2$) do not allow the computation of spatial distributions of the main plasma parameters via 2D self-consistent simulations [41].

3.1.2. Modelling results

The presented model for argon microwave plasma at reduced pressure allows for assessment of the spatial distribution of the wave properties and the most relevant plasma parameters. Numerical calculations are carried out at the following process conditions: gas flow rate 0.1 l/min, inlet gas temperature 293 K, input microwave power 200 W, operating pressure 10 mbar, inner and outer radius of the reactor 0.002 m and 0.0025 m respectively, and reactor length 0.4 m, which match the operating conditions set experimentally for the plasma ignition phase. Fig. 3 displays the deposited power over time for both reactor configurations. Fig. 4 presents the gas temperature and radial power flow, whereas Fig. 5 shows the spatially-resolved electric field distribution, electron density and electron temperature. The results given on the left-hand side of Fig. 4 and Fig. 5 correspond to Case 1 (no waveguide), while the results on the right-hand side correspond to the reactor configuration with the waveguide.

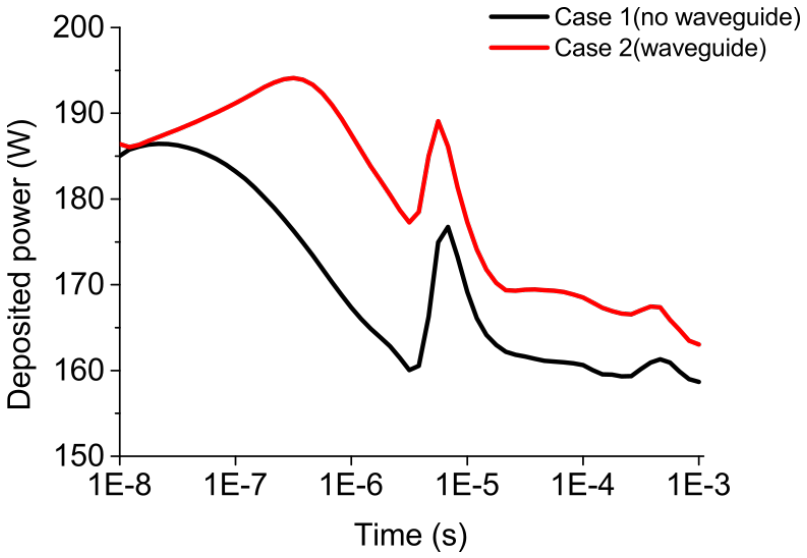

Fig. 3. Deposited microwave power over time for Case 1 (no waveguide) and Case 2 (waveguide).

Gas temperature: The main reactions responsible for heating of the gas in argon microwave plasma at reduced pressure are: (1) elastic scattering; electrons collide with neutral argon atoms causing no change in the internal energy of the colliding particles [42], and (2) two-body metastable quenching; excited argon atoms quench back to the ground state. Temperature gradients observed in the plasma volume are notably high due to very large L/R ratio (400/2 mm), where L is the length and R the radius of the reactor, as seen in Fig. 4(a); the temperature drops from ~1500 to 300 K within 30 mm. The maximum gas temperature calculated, although similar in both cases, is higher in Case 2 due to the higher deposited power (Fig. 3). This is also experimentally confirmed as discussed later in section "Optical Emission Spectroscopy analysis".

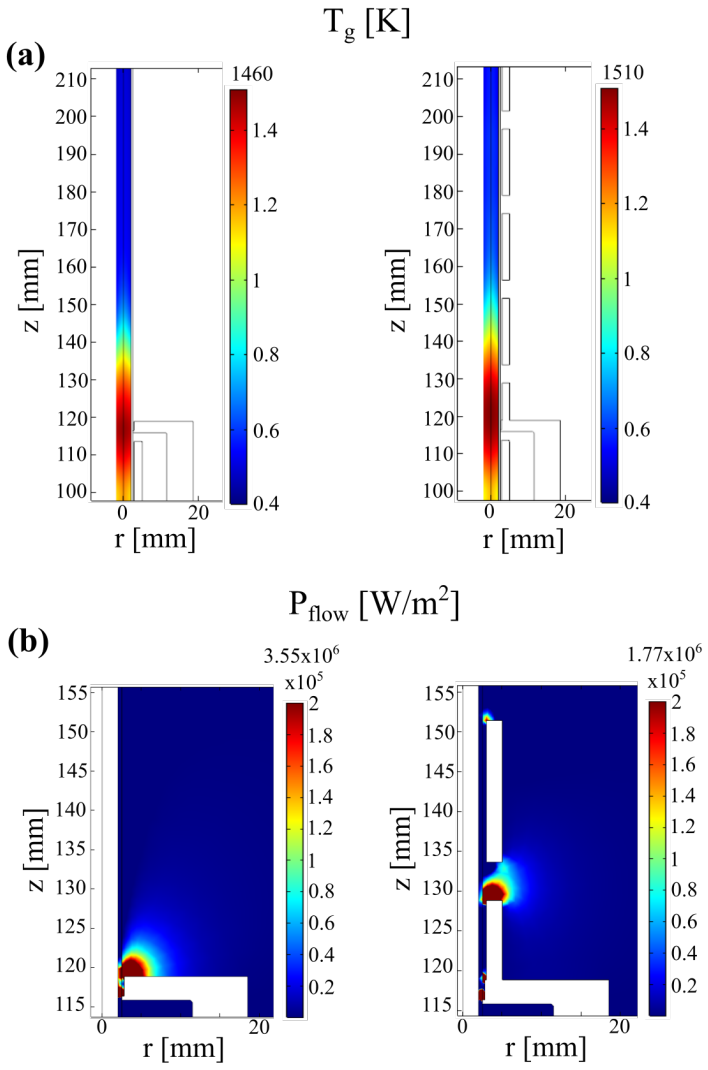

Fig. 4. Modelling results for both reactor configurations: Case 1, left-hand side (extended waveguide not included); Case 2, right-hand side (extended waveguide included). (a) gas temperature and (b) time-average ($t = 0\text{-}1 \cdot 10^{-3}$ s) radial power flow.

Electric field distribution: The electric field (wave) propagates along the z-direction due to the existence of the plasma; the plasma behaves as a waveguide, and simultaneously the plasma absorbs energy from the surface waves. As shown in Fig. 5(a-left), the electric field is concentrated in the free space surrounding the dielectric tube, right outside the wave launcher (z = 120 mm); this is also the region with the highest electron density [29] (see Fig. 5(b)). Regarding the case with the secondary waveguide (Case 2) in Fig. 5(a-right), the electric field is not concentrated at z = 120 mm, but rather at the first port that is used to measure the emission spectrum. This effect is also observed for the radial power flow in Fig. 4(b). Fig. 4(b-right) also shows that the power flow in the radial direction decreases in Case 2 (waveguide reactor), which implies reduction in power losses. The introduction of the cylindrical waveguide changes the E field and improves the uniformity of the deposited power over the plasma volume and therefore enlarges the plasma column. The maximum electric field is also altered by the waveguide due to the redistribution of power. Hence, the variation of the E field largely influences the plasma parameters, as wave properties, electron density (n_e), and electron temperature (T_e) are self-consistently related to each other [30].

Electron density: In the process of wave-to-plasma power coupling, the wave energy flux and the electron density decay along the discharge. As the wave propagates, a fraction of the wave energy is absorbed by the plasma column for its sustenance as far as the condition $n_e \geq n_{cr}$ is maintained; the critical plasma density at 2.45 GHz is $n_{cr} = 7.5 \cdot 10^{16}$ [$1/m^3$] [15]. Fig. 5(b) shows that the maximum electron density is higher in Case 2, as a consequence of a larger power density [19, 43] (see Fig. 3). It is also observed that the area with high electron density ($n_e > 1.4 \cdot 10^{20}$ [$1/m^3$]) values in the plasma is enlarged in the presence of the waveguide due to the increase in power absorption.

Electron temperature: Electron heating through collisions in the plasma volume takes place predominantly through the E_z –field component [18, 30]. As a consequence, the maximum electron temperature in Case 1 is higher compared to Case 2. The electric field has a direct dependence on the electron temperature [42] under the considered chemistry and conditions in the model. Nevertheless, as seen in Fig. 5(c), the spatial distribution of the electron temperature is more uniform in Case 2 as a result of the enhanced electric field distribution.

In conclusion, the proposed argon microwave plasma model allowed us to investigate the effect of an extended waveguide on the electromagnetic field distribution, the net input (deposited) microwave power, the key plasma parameters (n_e and T_e) and the gas temperature. We believe that the improvement on electron density and temperature uniformity in the discharge in combination with the gas temperature increase has the largest impact on the experimental results reported in the following section "Experimental work" for the RGWS reaction. From the engineering point-of-view, practical models, as the one presented herein, are of importance for further development of the microwave plasma (MWP) technology in general and alternative reactor configurations for improved process performance and scalability. The development of reduced kinetic models for key gas phase plasma chemistries, such as CO_2 splitting, RWGS ($CO_2 + H_2$) and dry reforming of methane ($CH_4 + CO_2$) is an important challenge in the plasma field [41].

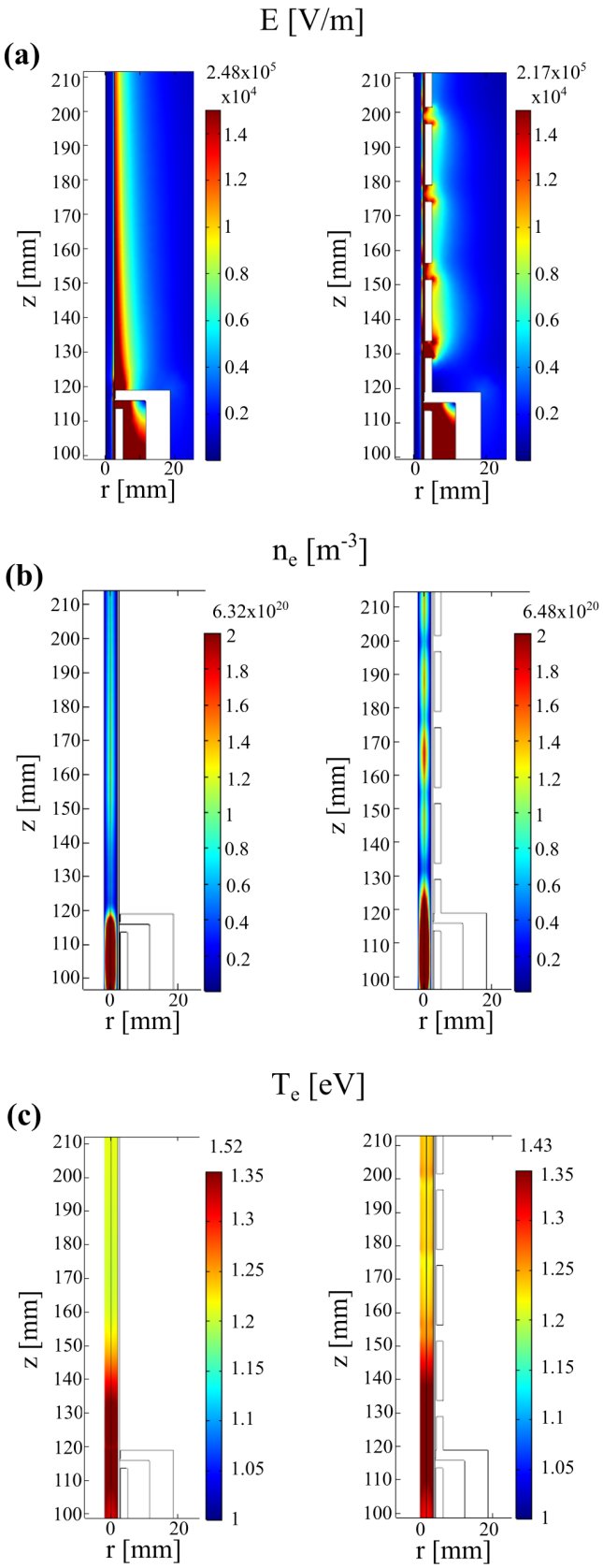

Fig. 5. Modelling results for both reactor configurations: Case 1, left-hand side (extended waveguide not included); Case 2, right-hand side (extended waveguide included). (a) electric field norm distribution, (b) electron density and (c) electron temperature.

3.2. Experimental work

In the previous section, a numerical model was proven to be a useful tool for the study of a process in alternative SW MWP reactor configurations. Research studies combining modelling and experimental work in MWP reactors are rather limited. In our previous work [27], we studied the RWGS reaction in a SW MWP reactor without an extended waveguide and reported CO_2 conversion up to 80% at a feed H_2:CO_2 ratio = 3. In this work, we carry out a detailed evaluation of the RWGS reaction in a novel reactor configuration involving an extended waveguide. To assess process performance, mass spectroscopy, optical emission spectroscopy and thermal imaging are used as analytical techniques, and the experimental results are presented in the following paragraphs.

3.2.1. Effect of the secondary waveguide on CO_2 conversion

With the aim of evaluating the RWGS reaction performance in two different reactor configurations, the operating conditions are kept constant in all the experiments. The inlet gas flow rate is maintained at 0.4 l/min, the net input microwave power at 150 W, and pressure at 25 mbar. The feed gas composition (H_2:CO_2) is varied from 1 to 3 (same as in our previous work [27]). The results presented in Fig. 6 shows that the addition of the waveguide leads to an improvement of about 50%, from 40% to 60%, on CO_2 conversion at a ratio H_2:CO_2 = 1. However, the effect is nearly negligible at higher ratios. To interpret the difference observed at ratio H_2:CO_2 = 1, the reader is referred to Fig. 7 in which the RWGS reaction is evaluated through a 0-D isothermal kinetic model [27]. At relatively low gas temperatures (1900-2100 K), the CO_2 conversion experiences large variations with small changes in gas temperature and/or the residence time. In Case 2, the waveguide increases the absorption of microwave power (Fig. 3 and Fig. 4) that leads to gas temperature rise (Fig. 4) and slight extension of the plasma column (residence time increase) (Fig. 4 and Fig. 5); this results in higher CO_2 conversion. The plasma generation system investigated in this work is a surface-wave launcher, so-called surfatron, which produces rather warm plasmas (2000-2500 K) within the category non-equilibrium discharges [44]. Even though the microwave discharge can be considered to be in non-equilibrium conditions due to the difference between electron temperature and gas temperature, presumably the dominant chemical reactions are thermally driven – that is, the CO_2 conversion improves when increasing the temperature of the bulk gas.

At higher ratios H_2:CO_2 ratios, this effect is no longer observed because in both cases, (i.e. with and without the waveguide), the gas temperature as well as the residence time are high enough to drive the CO_2 conversion to saturation on a shorter time scale, as displayed in Fig. 7 for H_2:CO_2 = 3. This finding is further evaluated in the following sections by means of OES.

When syngas is to be produced via the RWGS reaction, it is important to maximize the conversion of CO_2 to CO while using a minimum amount of H_2 as raw material, given that the production cost of H_2 is the main parameter driving the overall operating cost (OPEX) [10, 11, 45]. First, it is still expensive to manufacture H_2 via renewable energy-based production processes (electrolysis, plasma-assisted, photocatalysis) [46]. Second, low H_2:CO_2 feed ratios imply smaller MWP reactor volumetric footprint [47], which is beneficial given the current limited scalability of the MWP technology [48].

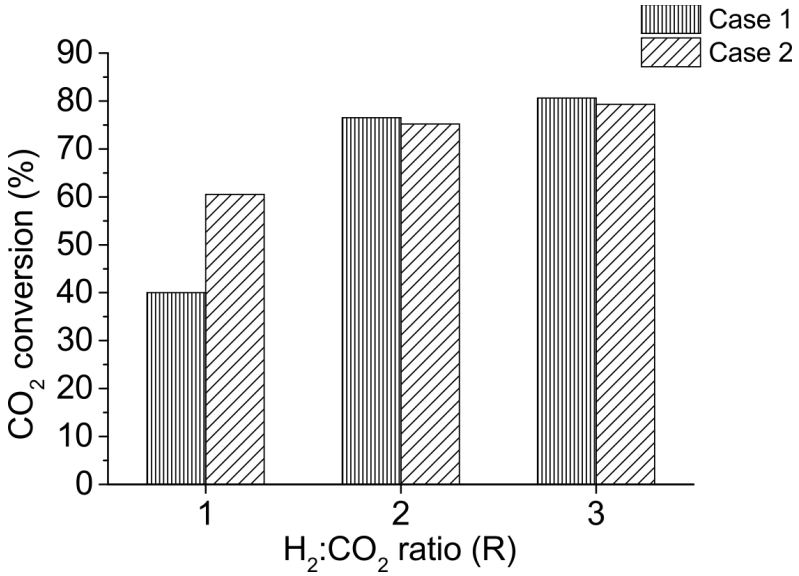

Fig. 6. Comparison of CO_2 conversion for two MWP reactor configurations: Case 1, extended waveguide not included; Case 2, extended waveguide included. Operating conditions: total gas flow rate = 0.4 l/min, net input microwave power = 150 W, operating pressure = 25 mbar.

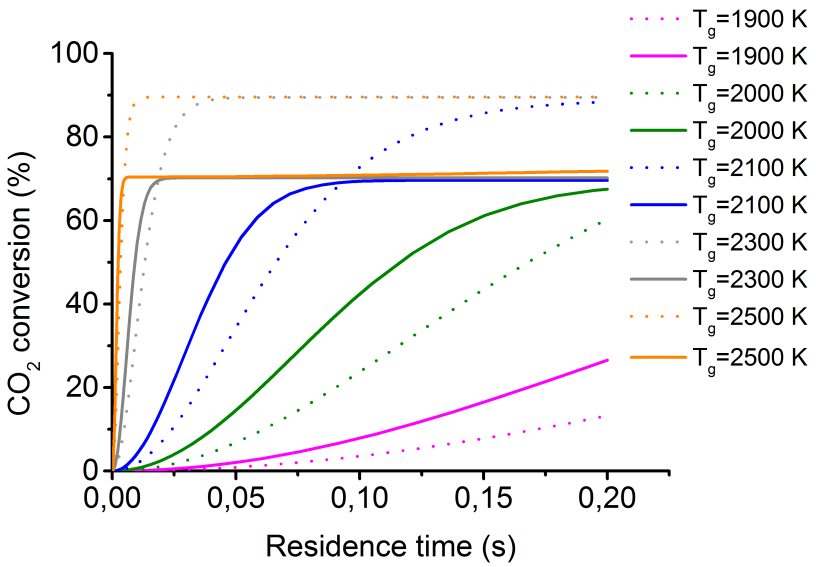

Fig. 7. Modelling results of RWGS reaction (CO_2 conversion) vs residence time at different gas temperatures (image reprinted with permission from [27]). Two feed gas mixture ratios are considered in the calculations; H_2:CO_2 = 1 (solid lines) and H_2:CO_2 = 3 (dot lines).

3.2.2. Optical Emission Spectroscopy (OES) analysis

To better understand the influence of the cylindrical waveguide on the SW microwave discharge, emission spectra obtained from the two MWP reactor configurations are analysed at different input microwave power values. Furthermore, the electron and gas temperatures are quantified by means of OES. In both cases, the measurements are taken 10 mm downstream from the surfatron launcher, where the first access port in the waveguide is located.

The emission line intensity is used to identify the relative quantities of the different excited species present in the plasma [49-52]. Fig. 8 highlights the changes observed in the concentration of key excited species when considering the two reactor configurations. It is clear that raising the input microwave power increases the production of reactive species, mainly OH radical, H and O atoms, as discussed in [53]. Notably, the concentration of OH radicals is larger in Case 1 (without waveguide), whereas the concentration of O atoms largely decreases in Case 1 as compared to Case 2 (waveguide reactor). This indicates that the CO_2 conversion process occurs faster in Case 2 due to the higher gas temperatures reached in the plasma; the higher concentration of O atoms is directly related to the degree of CO_2 dissociation. Based on the results, one can expect that the configuration of Case 2 (waveguide

reactor) would lead to higher CO_2 conversions, which indeed occurs at a feed ratio of H_2:CO_2 = 1 as displayed in Fig. 6. Hence, it is shown that the inclusion of an external element can alter the concentration of key excited species that dominate the plasma chemistry due to variations in wave and plasma properties, eventually leading to better reactor performance.

To further evaluate changes in the plasma parameters when adding a cylindrical waveguide to the MWP reactor, the electron temperature (T_e) and gas temperature (T_g) are calculated. We intended to estimate the electron density as well, but due to the low optical resolution of the employed spectrometer (> 1 nm FWHM), it was not possible to capture the H_β line at all feed ratios with enough data points to perform accurate fitting. The same methods used in our earlier work [27] are herein considered too for the determination of these parameters. In particular, T_e is determined based on its dependence on the atomic oxygen lines [26, 54, 55]. However, it should be noted that this method only provides rough estimations of T_e, therefore it is used to assess trends as to how operating process conditions influence plasma parameters and, consequently, the reactor performance. Concerning T_g, the detected OH radical [56] is used in the calculation process. The results obtained for the two reactor configurations are presented in Table 2. The values of T_e show a change in trend when comparing both cases, meaning that Case 2 shows a higher T_e than Case 1 at feed H_2:CO_2 = 1, whereas at higher ratios, Case 1 has higher T_e values. The electrons can be energized to higher values when the dissociation rate of the molecules increases; higher dissociation of CO_2 and H_2 molecules results in larger concentration of atomic species in the plasma, which cannot be excited vibrationally and/or rotationally by electrons. Due to the lack of energy transfer via vibrational and rotational excitation processes, electrons gain higher energies at a constant input microwave power, as seen in Table 2 for H_2:CO_2 = 1. The influence of the conversion rates on T_e for CO_2 splitting was also discussed by Kozak et al. [57], who showed that high power densities, which resulted in higher CO_2 conversions, led to lower T_e values due to variation in the species concentrations.

Table 2. Electron temperature (T_e) and gas temperature (T_g) for both reactor configurations. Operating conditions: total gas flow rate = 0.4 l/min, net input microwave power = 150, operating pressure = 25 mbar.

	CASE 1 = NON-WAVEGUIDE		CASE 2 = WAVEGUIDE	
T_e [Ev]	H_2:CO_2 = 1	1.43	H_2:CO_2 = 1	1.72
	H_2:CO_2 = 2	1.75	H_2:CO_2 = 2	1.73
	H_2:CO_2 = 3	1.96	H_2:CO_2 = 3	1.81
T_g [K]→(OH)	H_2:CO_2 = 1	2191	H_2:CO_2 = 1	2576
	H_2:CO_2 = 2	2382	H_2:CO_2 = 2	2687
	H_2:CO_2 = 3	2446	H_2:CO_2 = 3	2702

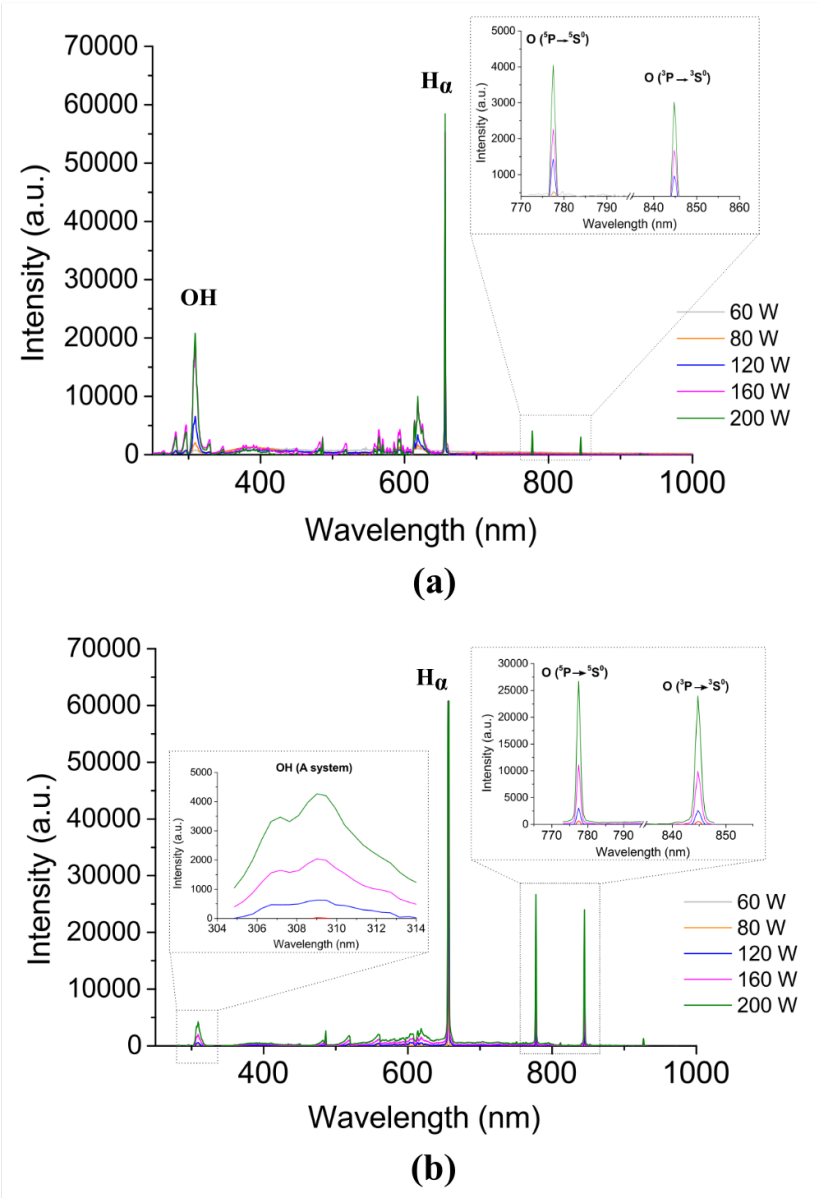

Fig. 8. Emission spectra at different input microwave power for (a) Case 1, waveguide not included and (b) Case 2, waveguide included. Operating conditions: total gas flow rate = 0.4 l/min, feed composition H_2:CO_2 = 1, operating pressure = 25 mbar.

However, the opposite behaviour is observed at higher H_2:CO_2 ratios where the concentration of H_2 is well in excess of the concentration of CO_2. The gas mixture change makes the H_2 chemistry dominate over the CO_2-related chemical processes. As stated by Hassouni et al. [43], in pure H_2 microwave discharges, the energy transfer channels highly depend on the considered discharge conditions. At low-power density, the predominant energy dissipation channel is through electron-impact H_2 dissociation, whereas at high-power density, a large fraction of the energy is dissipated in elastic collisions (~3 times higher than that dissipated through H_2 dissociation). At high H_2:CO_2 ratios, the power density is higher when the waveguide is included (Fig. 3), meaning that more energy is lost via elastic collisions yielding lower T_e values compared to the single discharge tube case (see Table 2). As the gas temperature increases, especially at the highest ratio (H_2:CO_2 = 3), the variation of T_e in Case 2 (waveguide reactor; T_e = 1.81 eV) versus that in Case 1 (single plasma tube-no waveguide; T_e=1.96 eV) shows that the plasma evolves faster from non-equilibrium towards thermal plasma conditions when the waveguide is present. Additionally, we should note that the electron density strongly depends on the power density [30, 58] and the H_2 content [27, 59]. Hence, higher electron density values are expected in the waveguide case and at high H_2 feed concentrations.

Regarding gas temperature T_g, the waveguide enhances the absorption of microwave power, which results in bulk gas temperature rise [19, 60], as shown in Table 2. The gas temperatures reported herein are mainly intended to draw conclusions from a qualitative perspective considering that these values are likely overestimated due to the lack of sufficient data points for a good fitting [27]. Nevertheless, the trends show that the largest difference is found at H_2:CO_2 = 1, where the thermal conductivity of the gas mixture has its minimum, i.e. the thermal conductivity of CO_2 is roughly 8 times lower than that of H_2. When H_2 is fed in excess (H_2:CO_2 > 1), the thermal conductivity of the plasma increases causing a more uniform gas temperature distribution and lower gas temperature differences between the two reactor configurations (18%, 13%, 10% for H_2:CO_2 = 1-3, respectively).

3.2.3. Infrared imaging

Thermography or infrared thermal imaging is a commonly used plasma diagnostics technique in fusion research [41-43]. Infrared radiation (IR) is emitted by all objects, and the amount of

radiation increases with temperature. The radiative properties of a body are denoted by the emittance or emissivity (ε), which changes with temperature. In this work, the IR camera is used for the identification of the plasma length along with the dissociation and recombination zones (Fig. 9). As stated by Fridman et al. [42], molecules are mostly dissociated into atoms in a zone with higher temperature and are much less dissociated in lower-temperature zones. Therefore, in Fig. 9, the IR camera enables us to visualize the effect of the feed H_2:CO_2 ratio on the plasma, i.e. the dissociation or high temperature zone (whitish) and the recombination or low temperature zone (bluish) [61, 62]. Fig. 9 shows clearly how the dissociation zone is enlarged and the recombination zone is shrunk when increasing the feed ratio H_2:CO_2 from 1 to 3. At feed ratio 4, the difference is barely noticeable. This also agrees with the fact that H_2 presents much larger thermal conductivity compared to CO_2; thus the increase in the H_2 content should result in enlargement of the high temperature zone in combination with greater plasma uniformity [42, 44, 59, 63]. This explains the higher CO_2 conversions obtained at high H_2:CO_2 ratios.

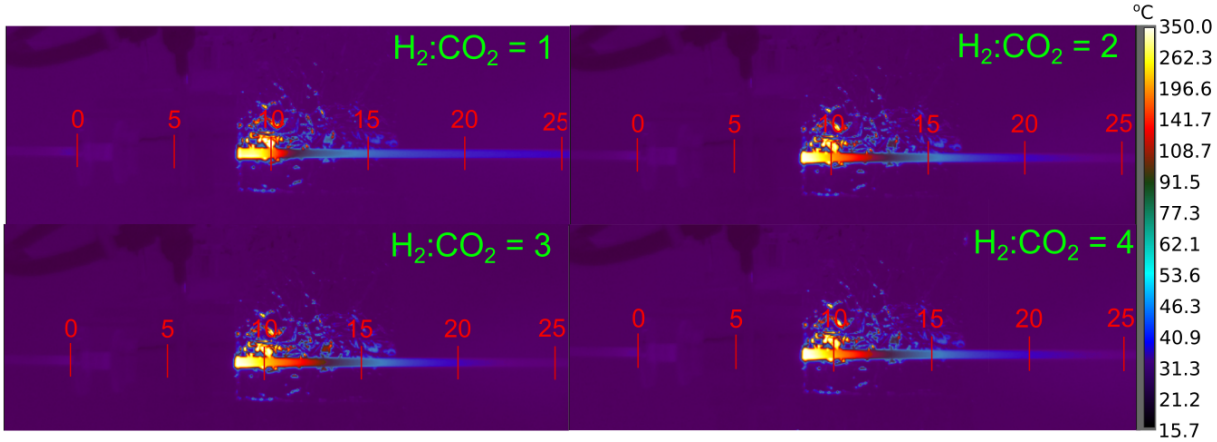

Fig. 9. Thermal images of the plasma reactor (Case 1, waveguide not included) at different feed H_2:CO_2 ratios. The dimensions specified in the Figure (red colour numbers) are in cm scale. The temperature scale on the left is calculated considering an emissivity of quartz equal to 0.9. These values do not represent the gas plasma temperature, but rather a rough estimation of the surface plasma/inner reactor wall temperature. Operating conditions: total gas flow rate = 0.4 l/min, net input microwave power = 150, operating pressure = 25 mbar.

3.2.4. Effect of other process parameters on CO_2 conversion

The effects of operating pressure and cooling N_2 flow rate on CO_2 conversion are assessed. The operating pressure defines how close or far from thermal equilibrium plasma is, as it

influences directly the electron-neutral collision frequency and therefore the energy transferred from the electrons to the bulk gas. As reported by Fridman et al. [42], the optimum pressure range for plasma-chemical applications in microwave discharges lies in the range 20-200 mbar. At relatively low pressures (20-70 mbar), the diffusive regime prevails in the plasma; the discharge is attached to the wall (expanded-like plasma), whereas at intermediate pressures (70-200 mbar), the combined regime takes place in which a contraction of the discharge is observed (contracted-like plasma). The experimental results in Fig. 10(a) show that there is a minimum CO_2 conversion at ~75 mbar. It appears that this minimum is presented at the transition point, where the plasma evolves from a diffusive to a combined regime.

We measured the emission spectra at three different pressures within the diffusive regime (22, 44, 66 mbar) to gain insight into how the operating pressure influences the chemical species present in the plasma. Fig. 10(b) shows that increase in pressure (up to 66 mbar) decreases the concentration of reactive species (OH radical, H and O atoms), which drive the RWGS reaction in the plasma. As already mentioned, the generation of O atoms is directly linked to the CO production rate. Belete et al. [53] studied the direct dissociation of CO_2 and H_2O for syngas production in a microwave plasma reactor, showing that a higher operating pressure in the diffusive regime results in lower generation of excited species, as seen in Fig. 10(b) for the RGWS reaction.

Another important parameter is the cooling N_2 flow rate. The effect of the cooling water is also evaluated, although it has no measurable effect on the reactor performance. The cooling N_2 flow rate, meant to cool down the quartz tube, affects significantly the CO_2 conversion as outlined in Fig. 11. While CO_2 conversion is ~35% at low N_2 flow rates, it drops down to ~15% when the N_2 flow rate is increased to 40 l/h. This is also noticed visually during the experiments, where the increase in the N_2 flow rate shrinks the dissociation (brightest) zone in the plasma. Note that to sustain plasma with no N_2 cooling, the input microwave power has to be lowered considerably in order not to melt the quartz tube. This represents a compromise between the integrity of the MWP reactor and its performance. Therefore, careful design of the cooling system to avoid reactor melting while optimizing the plasma potential is required when developing MWP technology.

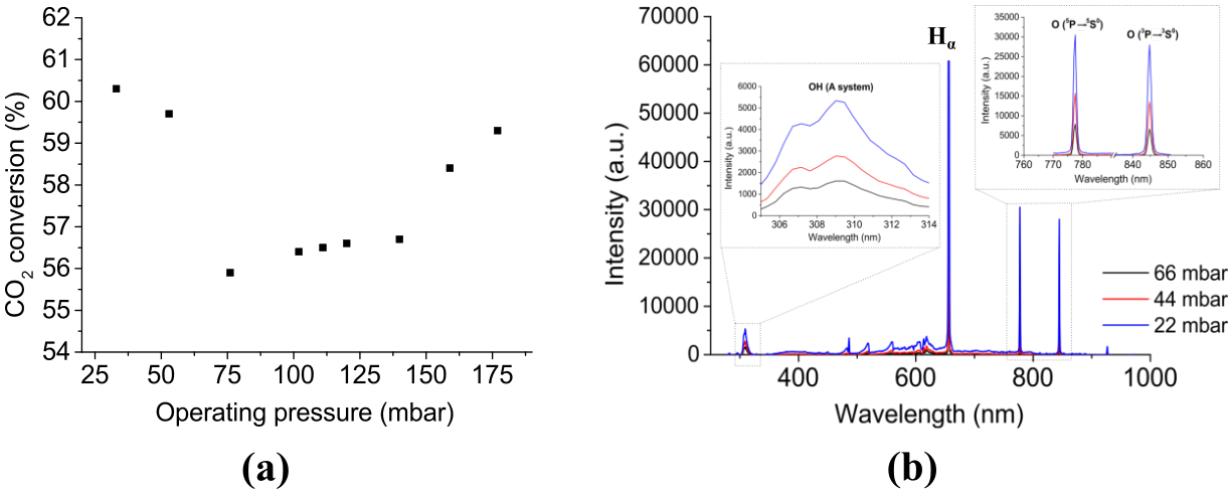

Fig. 10. (a) Effect of operating pressure on CO_2 conversion and (b) the emission spectra at three different pressures, for Case 2 (waveguide included). Operating conditions: total gas flow rate = 0.4 l/min, feed gas composition H_2:CO_2 = 1, net input microwave power = 150 W.

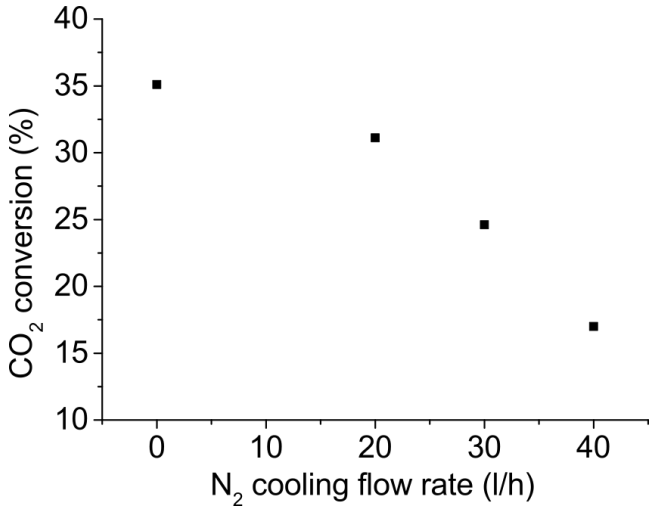

Fig. 11. Effect of the cooling N_2 flow rate on CO_2 conversion for Case 2 (waveguide included). Operating conditions: total gas flow rate = 0.4 l/min, feed composition H_2:CO_2 = 1, net input microwave power = 80 W, operating pressure = 25 mbar.

4. Conclusions

A novel surface wave-sustained microwave discharge reactor configuration was numerically and experimentally investigated to improve CO_2 conversion to CO through the reverse water gas-shift reaction in gas phase. We developed a 2D axisymmetric self-consistent model of argon microwave plasma to study the influence of a cylindrical waveguide on the electric field distribution, key plasma parameters, and gas temperature. The modelling results show

that the waveguide increases the absorption of microwave power by the plasma, which in turn increases the gas temperature. The spatial uniformity of the electron density and electron temperature is improved as well in the presence of the waveguide. We proved experimentally that the waveguide changes the plasma reactor performance. CO_2 conversion increase by 50%, from 40% to 60%, is achieved for the stoichiometric feed gas composition ratio H_2:CO_2 = 1 when the waveguide is present. At higher feed ratios, the effect of the waveguide is nearly negligible. Increase in H_2 content in the feed (H_2:CO_2 > 1) causes a rise in gas temperature and residence time, which drive the dissociation of CO_2 to saturation on a shorter time scale as compared to the case of H_2:CO_2 = 1. Furthermore, the formation of other carbon-bearing products (e.g. methane, methanol) was analysed throughout all the experiments. It was observed that negligible amounts of these species are formed, implying that nearly 100% selectivity of CO_2 to CO is achieved.

We also studied how the operating pressure in the range 20-200 mbar and the cooling N_2 flow rate influence the reactor performance. The CO_2 conversion presents a minimum at ~75 mbar, which might be related to the change in the plasma operating regime from diffusive to contracted mode. The effect of the cooling N_2 flow rate on CO_2 conversion is remarkably high, meaning that careful design of the cooling system is required to optimize plasma efficiency.

Acknowledgements

This research was supported by Alternative Energy Forms for Green Chemistry (ALTEREGO), a European cooperation project funded within the 7th Framework Programme with grant agreement No. 309874. We would like to acknowledge Guido Sturm (TU Delft) for the technical support in the design and development of the setup, Lennart Middelplaats (TU Delft) for his contribution on the implementation of the LabVIEW interface, and also the technicians from DEMO (Gerard, Bas, Martijn-TU Delft) who participated in the construction of the setup.

References

[1] International Energy Agency (IEA) Energy Balances U.S. Final Energy Consumption 2012.

[2] Pearson RJ, Eisaman MD, Turner JWG, Edwards PP, Jiang Z, Kuznetsov VL, et al. Energy Storage via Carbon-Neutral Fuels Made From CO2, Water, and Renewable Energy. P Ieee. 2012;100:440-60.

[3] Goeppert A, Czaun M, Jones JP, Prakash GKS, Olah GA. Recycling of carbon dioxide to methanol and derived products - closing the loop. Chem Soc Rev. 2014;43:7995-8048.

[4] Varne M, Dey GR, Das TN. Evaluation of optimum conditions for hydrogen generation in argon-water vapor dielectric barrier discharge. Int J Hydrogen Energ. 2016;41:22769-74.

[5] Banerjee S, Musa MN, Jaafar AB. Economic assessment and prospect of hydrogen generated by OTEC as future fuel. Int J Hydrogen Energ. 2016.

[6] Du C, Ma D, Wu J, Lin Y, Xiao W, Ruan J, et al. Plasma-catalysis reforming for H2 production from ethanol. Int J Hydrogen Energ. 2015;40:15398-410.

[7] Levin DB, Chahine R. Challenges for renewable hydrogen production from biomass. Int J Hydrogen Energ. 2010;35:4962-9.

[8] Kranenburg Kv, Schols E, Gelevert H, Kler Rd, Delft Yv, Weeda M. Empowering the chemical industry: Opportunities for electrification. 2016:1-32.

[9] Mennicken L, Janz A, Roth S. The German R&D Program for CO2 Utilization-Innovations for a Green Economy. Environ Sci Pollut R. 2016;23:11386-92.

[10] Lim XZ. How to make the most of carbon dioxide (vol 526, pg 628, 2015). Nature. 2016;529:141-.

[11] Centi G, Perathoner S. Green carbon dioxide: Advances in CO2 utilization: Wiley; 2014.

[12] Peter M. Maitlis, Arno de Klerk. Greener Fischer-Tropsch processes for fuels and feedstocks: Wiley; 2013.

[13] Czylkowski D, Hrycak B, Miotk R, Jasiński M, Dors M, Mizeraczyk J. Hydrogen production by conversion of ethanol using atmospheric pressure microwave plasmas. Int J Hydrogen Energ. 2015;40:14039-44.

[14] Jasiński M, Czylkowski D, Hrycak B, Dors M, Mizeraczyk J. Atmospheric pressure microwave plasma source for hydrogen production. Int J Hydrogen Energ. 2013;38:11473-83.

[15] Schulz A, Buchele P, Ramisch E, Janzen O, Jimenez F, Kamm C, et al. Scalable Microwave Plasma Sources From Low to Atmospheric Pressure. Contrib Plasm Phys. 2012;52:607-14.

[16] Lebedev YA. Microwave discharges: generation and diagnostics. 25th Summer School and International Symposium on the Physics of Ionized Gases - Spig 2010. 2010;257.

[17] Ferreira CM, Moisan M. Microwave Discharges Fundamentals and Applications: NATO ASI Series; 1993.

[18] Schluter H, Shivarova A. Travelling-wave-sustained discharges. Phys Rep. 2007;443:121-255.

[19] Georgieva V, Berthelot A, Silva T, Kolev S, Graef W, Britun N, et al. Understanding Microwave Surface-Wave Sustained Plasmas at Intermediate Pressure by 2D Modeling and Experiments. Plasma Process Polym. 2016:n/a-n/a.
[20] Chen G, Silva T, Georgieva V, Godfroid T, Britun N, Snyders R, et al. Simultaneous dissociation of CO2 and H2O to syngas in a surface-wave microwave discharge. Int J Hydrogen Energ. 2015;40:3789-96.
[21] Henriques J, Bundaleska N, Tatarova E, Dias FM, Ferreira CM. Microwave plasma torches driven by surface wave applied for hydrogen production. Int J Hydrogen Energ. 2011;36:345-54.
[22] Nizio M, Albarazi A, Cavadias S, Amouroux J, Galvez ME, Da Costa P. Hybrid plasma-catalytic methanation of CO2 at low temperature over ceria zirconia supported Ni catalysts. Int J Hydrogen Energ. 2016;41:11584-92.
[23] Bongers W, Bouwmeester H, Wolf B, Peeters F, Welzel S, van den Bekerom D, et al. Plasma-driven dissociation of CO2 for fuel synthesis. Plasma Process Polym. 2016:n/a-n/a.
[24] van Rooij G, van den Bekerom D, den Harder N, Minea T, Berden G, Bongers W, et al. Taming microwave plasma to beat thermodynamics in CO2 dissociation. Faraday Discuss. 2015;183:233-48.
[25] Bhattacharya M, Basak T. A theoretical study on the use of microwaves in reducing energy consumption for an endothermic reaction: Role of metal coated bounding surface. Energy. 2013;55:278-94.
[26] Spencer LF. The Study of CO2 Conversion in a Microwave Plasma/Catalyst System. 2012;PhD Thesis University of Michigan.
[27] de la Fuente JF, Moreno SH, Stankiewicz AI, Stefanidis GD. Reduction of CO2 with hydrogen in a non-equilibrium microwave plasma reactor. Int J Hydrogen Energ. 2016;41:21067-77.
[28] Nguyen SVT, Foster JE, Gallimore AD. Operating a radio-frequency plasma source on water vapor. Rev Sci Instrum. 2009;80.
[29] Selby M, Hieftje GM. Taming the Surfatron. Spectrochim Acta B. 1987;42:285-98.
[30] Schluter H, Shivarova A. Advanced technologies based on wave and beam generated plasmas: Springer Netherlands; 1999.
[31] COMSOL, Multiphysics, 5.1. Microwave Plasma Module User's Guide. COMSOL AB. 2015.
[32] Phelps database (www.lxcat.net/Phelps) retrieved from http://jilawww.colorado.edu/~avp/.
[33] Hyman HA. Electron-impact ionization cross sections for excited states of the rare gases (Ne, Ar, Kr, Xe), cadmium, and mercury. Phys Rev A. 1979;20:855-9.
[34] Karoulina EV, Yu AL. Computer simulation of microwave and DC plasmas: comparative characterisation of plasmas. Journal of Physics D: Applied Physics. 1992;25:401.
[35] Lymberopoulos DP, Economou DJ. Fluid simulations of glow discharges: Effect of metastable atoms in argon. J Appl Phys. 1993;73:3668-79.

[36] Ferreira CM, Loureiro J, Ricard A. Populations in the metastable and the resonance levels of argon and stepwise ionization effects in a low-pressure argon positive column. J Appl Phys. 1985;57:82-90.
[37] Jimenez-Diaz M, Carbone EAD, van Dijk J, van der Mullen JJAM. A two-dimensional Plasimo multiphysics model for the plasma-electromagnetic interaction in surface wave discharges: the surfatron source. J Phys D Appl Phys. 2012;45:335204.
[38] Baeva M, Bosel A, Ehlbeck J, Loffhagen D. Modeling of microwave-induced plasma in argon at atmospheric pressure. Phys Rev E. 2012;85:056404.
[39] Xiao W, Huang KM, Zhang WC, Lin Y. Modeling of Argon Plasma Excited by Microwave at Atmospheric Pressure in Ridged Waveguide. Ieee T Plasma Sci. 2016;44:1075-82.
[40] Obrusnik A, Bonaventura Z. Studying a low-pressure microwave coaxial discharge in hydrogen using a mixed 2D/3D fluid model. J Phys D Appl Phys. 2015;48.
[41] de la Fuente JF, Moreno SH, Stankiewicz AI, Stefanidis GD. A new methodology for the reduction of vibrational kinetics in non-equilibrium microwave plasma: application to CO2 dissociation. Reaction Chemistry & Engineering. 2016;1:540-54.
[42] Fridman A. Plasma Chemistry: Cambridge: Cambridge University Press; 2008.
[43] Hassouni K, Gicquel A, Capitelli M, Loureiro J. Chemical kinetics and energy transfer in moderate pressure H-2 plasmas used in diamond MPACVD processes. Plasma Sources Sci T. 1999;8:494-512.
[44] Jankowski KJ, Reszke E. Microwave Induced Plasma Analytical Spectrometry: RSCPublishing 2011.
[45] Harmsen J. Industrial Process Scale-up: A practical innovation guide from idea to commercial implementation: Elsevier; 2013.
[46] Dincer I, Acar C. Review and evaluation of hydrogen production methods for better sustainability. Int J Hydrogen Energ. 2015;40:11094-111.
[47] Kaiser M, Baumgartner KM, Mattheus A. Microwave Plasma Sources -Applications in Industry. Contrib Plasm Phys. 2012;52:629-35.
[48] de la Fuente JF, Kiss AA, Radoiu MT, Stefanidis GD. Microwave plasma emerging technologies for chemical processes. Journal of Chemical Technology & Biotechnology. 2017:n/a-n/a.
[49] Chen GX, Silva T, Georgieva V, Godfroid T, Britun N, Snyders R, et al. Simultaneous dissociation of CO2 and H2O to syngas in a surface-wave microwave discharge. Int J Hydrogen Energ. 2015;40:3789-96.
[50] Belmonte T, Noel C, Gries T, Martin J, Henrion G. Theoretical background of optical emission spectroscopy for analysis of atmospheric pressure plasmas. Plasma Sources Sci T. 2015;24.
[51] Miotk R, Jasinski M, Mizeraczyk J. Optical emission spectroscopy of plasma generated by a waveguide-supplied microwave plasma source operated at 915MHz. Phys Scripta. 2014;T161.

[52] Laux CO, Spence TG, Kruger CH, Zare RN. Optical diagnostics of atmospheric pressure air plasmas. Plasma Sources Sci T. 2003;12:125-38.
[53] Belete TT, Van de Sanden MCM, Gleeson MA. Plasma dissociation of water for CO2 conversion. 22nd International Symposium on Plasma Chemistry. 2015.
[54] O'Connor N, Humphreys HH, Daniels S. Oxygen line ratio method for the determination of plasma parameters in atmospheric pressure discharges using air as the working gas. 31st ICPIG, Granada, Spain. 2013.
[55] Leins M, Walker M, Schulz A, Schumacher U, Stroth U. Spectroscopic Investigation of a Microwave-Generated Atmospheric Pressure Plasma Torch. Contrib Plasm Phys. 2012;52:615-28.
[56] Silva T, Britun N, Godfroid T, Snyders R. Optical characterization of a microwave pulsed discharge used for dissociation of CO2. Plasma Sources Sci T. 2014;23:025009.
[57] Kozak T, Bogaerts A. Splitting of CO2 by vibrational excitation in non-equilibrium plasmas: a reaction kinetics model. Plasma Sources Sci T. 2014;23:045004.
[58] Hassouni K, Silva F, Gicquel A. Modelling of diamond deposition microwave cavity generated plasmas. J Phys D Appl Phys. 2010;43.
[59] Leins M, Kopecki J, Gaiser S, Schulz A, Walker M, Schumacher U, et al. Microwave Plasmas at Atmospheric Pressure. Contrib Plasm Phys. 2014;54:14-26.
[60] den Harder N, van den Bekerom DCM, Al RS, Graswinckel MF, Palomares JM, Peeters FJJ, et al. Homogeneous CO2 conversion by microwave plasma: Wave propagation and diagnostics. Plasma Process Polym. 2016:n/a-n/a.
[61] Kwak HS, Uhm HS, Hong YC, Choi EH. Disintegration of Carbon Dioxide Molecules in a Microwave Plasma Torch. Sci Rep-Uk. 2015;5:18436.
[62] Choi DH, Chun SM, Ma SH, Hong YC. Production of hydrogen-rich syngas from methane reforming by steam microwave plasma. J Ind Eng Chem. 2016;34:286-91.
[63] Kopecki J. Developement and spectroscopic investigastions on a microwave plasma torch for the deposition process with powders. 2012;Doctoral Thesis University of Stuttgart.